Kinetics of Protein Deposition and Replacement from a Shear Flow

E. Mandrusov, J. D. Yang, N. Pfeiffer, L. Vroman, E. Puszkin, and E. F. Leonard
Artificial Organs Research Laboratory, Dept. of Chemical Engineering, Materials Science, and Mining Engineering, Columbia University, New York, NY 10027

Kinetics of plasma protein deposition and replacement from a shear flow of full strength and diluted blood plasma onto prewetted glass were studied both numerically and experimentally. A band of fibrinogen moving down the adsorbing surface was predicted and observed. The band was shown to define the region where blood platelets subsequently adhered to the surface. Since platelet adhesion is a fundamental component of thrombosis, this observation is potentially pertinent to the long-sought mechanism that determines where thrombus forms during shear flow of blood through artificial devices. The discrepancies between the mathematical model and experimental observations are explained by the presence of the natural convection, arising from density differences between plasma and the wetting fluids.

Introduction

The interaction of blood with artificial materials has limited and influenced the development of artificial organs and cardiovascular implants over the whole history of such devices. The most important and undesirable outcome of blood–material interaction is the formation of thrombi (adherent masses) and emboli (masses released into the fluid stream). Thrombi and emboli are the product of two reacting systems, a cascade of protein reactions that results in the insoluble polymer fibrin and a series of transformations of blood platelets that result in the formation of platelet layers, plugs, and microemboli. The protein and platelet reaction systems stimulate each other. No material, anticoagulant, or flow channel design has yet completely abrogated the formation of thrombi and emboli. Contemporary devices perform better than their predecessors but only as a result of the evolution of materials, therapeutic regimens, and design. Much more is known about particular steps in the thromboembolitic process, and the present study is a modest effort to bridge the gap between rather complete knowledge of some steps and the incapacity to predict when and where thrombogenesis will occur. It applies an established theory of protein deposition from plasma onto artificial materials to a simple flow situation encountered in almost all devices.

Correspondence concerning this article should be addressed to E. F. Leonard.

In clinical practice the first blood that contacts an artificial surface is diluted due to the presence of an incubating solution (in which the device has been rinsed before use). Blood plasma proteins deposit onto the surface of the device and undergo surface reactions slower than they would if the blood carrying them were not being diluted.

Blood proteins deposit on artificial surfaces sequentially. A phenomenon known as the Vroman effect is manifested when albumin, the most prevalent blood plasma protein, adsorbs first, and is then replaced by immunoglobulin-G (IgG), which is replaced by fibrinogen (Fg), and finally by high-molecular-weight kininogen (HMK) (Vroman and Adams, 1986; Vroman et al., 1980). The amount of Fg adsorbed from plasma on artificial surfaces depends on exposure time, plasma dilution, material surface properties, buffer composition, and temperature. It has been shown that on hydrophobic surfaces proteins other than HMK may play a central role in Fg displacement (Slack and Horbett, 1995). In this and other studies on hydrophilic surfaces the appearance of HMK correlates with the disappearance of Fg. Of the proteins in the Vroman effect, Fg is particularly reactive with blood platelets. In the time between Fg deposition and its replacement by HMK, platelet adhesion and activation take place. We have previously ascertained that the Vroman effect is prolonged on prewetted surfaces bounded by separated flows (Mandrusov et al., 1996b; LeDuc et al., 1994). We have also demon-

strated that Fg, deposited on the glass surface as a component of the adsorption sequence, is capable of binding and activating resting platelets. The work reported here deals with these effects at the boundaries of shear flows. Specifically, it reports on the existence of an Fg band, which moves along the surface of a flow channel in a manner dependent on the shear rate, and it rationalizes the moving band of Fg in terms of the Vroman effect.

Experimental studies of the Vroman effect on glass surfaces

After the phenomenon of sequential protein deposition was observed by Vroman, it was further studied by many others. The rate of protein displacement was shown to be limited either by diffusion of the molecules to the surface or by the surface reaction itself. Wojciechowski et al. (1986) exposed dilute plasma to the inner surfaces of glass tubes under static conditions (buffer initially filling the tubes was displaced by plasma using about 20 tube volumes) and observed that the initial protein adsorption was diffusion-limited. In a similar study, Wojciechowski and Brash (1991) showed a small axial dependence on deposition, presumably due to a boundary layer of varying thickness established by the plasma-loading technique. Cornelius et al. (1992) studied plasma protein adsorption to glass in a well-stirred system, and reported two "regimes" of initial rapid adsorption followed by a regime of slower adsorption; the principal adsorption rate limitation was due to protein supply and the kinetics of surface binding. Diffusion effects were shown to be negligible in a well-stirred system. Boumaza et al. (1992) performed a continuous kinetic study of the adsorption of Fg out of a single protein solution onto the inner surface of a glass tube under shear, measuring Fg deposition in a 2-cm-long section located at the center of a 10-cm glass capillary. For this segment, the diffusion coefficient required to fit data to a steady-state, convective-diffusion model was determined to be very close to the theoretical value reported in the literature. Wojciechowski and Brash (1991) have reported that the Vroman effect is accelerated by convection and limited by diffusion during shear flow. No previous report describes both the spatial and temporal variations of Fg adsorbed from plasma in shear flow.

Modeling of the Vroman effect

Different aspects of the Vroman effect have been modeled, both in static and shear-flow systems. Wojciechowski and Brash (1990) have modeled Fg adsorption from a static fluid. They employed a computer simulation to solve a steady-state diffusion equation, whose boundary conditions describe adsorbate kinetics in terms of two adsorbed states for Fg. Lu et al. (1994) have described sequential adsorption of albumin, IgG, and Fg, assuming steady-state diffusion kinetics that take into account two adsorbed states for each type of adsorbed molecule. Dejardin et al. (1995) have developed a kinetic model in which initially adsorbed Fg can either desorb spontaneously, relax to an irreversibly bound state, or exchange with HMK. They used the steady-state convective-diffusion model to predict the diffusion coefficients for a Langmuirian kinetic model. LeDuc et al. (1995) have modeled the adsorption of albumin, Fg, and HMK in a static fluid, taking into account more than two adsorbed states for one or more molecular species and also allowing for desorption from the second state when dissolved sorbent molecules are present. Slack and Horbett (1989) have modeled the kinetics of Fg adsorption and displacement from a static fluid, neglecting mass-transfer limitations and treating plasma as a binary mixture of Fg and another hypothetical protein (that displaces it). Fg was allowed to exist in two different bound states—weakly and tightly bound. Dejardin has also addressed the problem of a single protein adsorbing out of a flowing solution (Dejardin, 1989; Yan and Dejardin, 1991). His model assumes a quasi-steady-state regime near the interface to solve the two-dimensional convective-diffusion equation at steady state.

Thus far, experimental studies of the Vroman effect have been limited to the static systems or steady-state shear-flow systems, where both concentration and velocity profiles are fully developed. The work presented here investigates the Vroman effect under unsteady-state conditions—while the velocity profile is fully developed, the concentration profile is developing as blood plasma is introduced into a saline-filled channel. The process of deposition and removal of both Fg and HMK out of plasma during shear flow is traced spatially and temporally, over the entire surface of the channel, using a quantitative staining technique developed in the authors' laboratory (Mandrusov et al., 1996a). This article presents the first evidence that a band of Fg moves down the adsorbing surface with time, and a simple model that employs a transient convective diffusion equation to calculate the time and location of the arrival of Fg and the HMK is developed. Both numerical and experimental results indicate that the temporal and spatial window in which Fg is present on the surface is large and significant. The Fg stains are compared to those of adhered platelets, and are found to be nearly identical. The presented data implicates the prolonged residence time of Fg on a surface, caused by plasma dilution, as an inducer of platelet binding and activation, and implies that this process is an initiator of thrombogenesis.

Experimental Materials and Methods

All experiments and material preparations are done at room temperature

Materials. Distilled water, passed through a Millipore CDMF01204 Milli-Q system, is utilized for the preparation of all reagents. Normal saline, used to dilute plasma, contains 145-mM sodium chloride. The modified Tyrode's buffer (pH 7.5), used for preparing platelet suspension, contains 136 mM sodium chloride, 2.7 mM potassium chloride, 4.6 mM sodium phosphate monobasic, 12 mM sodium bicarbonate, 0.4 mM magnesium chloride, 0.01% glucose, 10 mM HEPES (Sigma Chemicals, St. Louis), and 10^{-3} mg/mL apyrase (Sigma Chemicals, St. Louis). Coomassie blue dye, used for platelet staining, is made by suspending 250 mg of Brilliant Blue G (Sigma Chemicals, St. Louis) in 50 mL of methanol and 10 mL glacial acetic acid and then diluting this mixture to 100 mL with water.

Normal, human, intact plasma and platelet-rich plasma (PRP), obtained from blood collected in 15% citrate phosphate dextrose adenine (CPDA-1), was kindly donated by the

Bergen County Blood Bank (Paramus, NJ). Plasma was stored at −70°C and thawed immediately before use. PRP was used within 24 h of collection time. The platelets were tested for viability by monitoring their aggregation in a Payton 300b aggregometer after the suspension was challenged with 10^{-5} M ADP (Sigma Chemicals, St. Louis). Upon challenge, all platelets have aggregated within 1 min.

The platelet suspension is prepared from the PRP as follows: the pH of the PRP is adjusted to 6.5 with 0.11 M citric acid and the suspension is centrifuged for 15 min at 2,000 rpm. The plasma is decanted and the pellet of platelets is resuspended to the original plasma volume (1.0×10^5 cells per μL) in modified Tyrode's buffer. The platelets are allowed to equilibrate at room temperature for 30 min before the initiation of experiments.

Glass plates (30×6 cm) are cut out of 2-mm-thick (single-weight) window glass and cleaned by immersing in Chromerge Cleaning Solution (Fisher Scientific, Pittsburgh) for two hours. The plates are thoroughly rinsed in distilled water and equilibrated overnight in tris buffer (0.2 M, pH 7.2) (Sigma Chemicals, St. Louis). The immunospecific polystyrene beads are prepared as described previously (Mandrusov et al., 1996a).

A staining well is used for the exposure of the glass plates to the platelet suspensions. The well accommodates the glass plate and a 2.5-mm thickness of the platelet suspension above the glass surface.

Shear-Flow Chamber. The shear-flow chamber is illustrated in Figure 1. It consists of a top plate, a gasket, and a glass plate. The gasket is manufactured by a photoetching process, used for fabrication of rubber stamps. The channels are created when the rubber gasket is laid over the glass plate. The gasket defines four independent channels, each 25 cm long, with identical trapezoidal (almost rectangular) cross-sectional areas. The assembly of glass plate, gasket, and a top plate is sealed with 12 clamps. One channel of this assembly is used at a time. Plasma is supplied through a port located at the entrance of the channel by a syringe pump; saline in reverse flow is supplied through the port located at the end of the channel by a peristaltic pump.

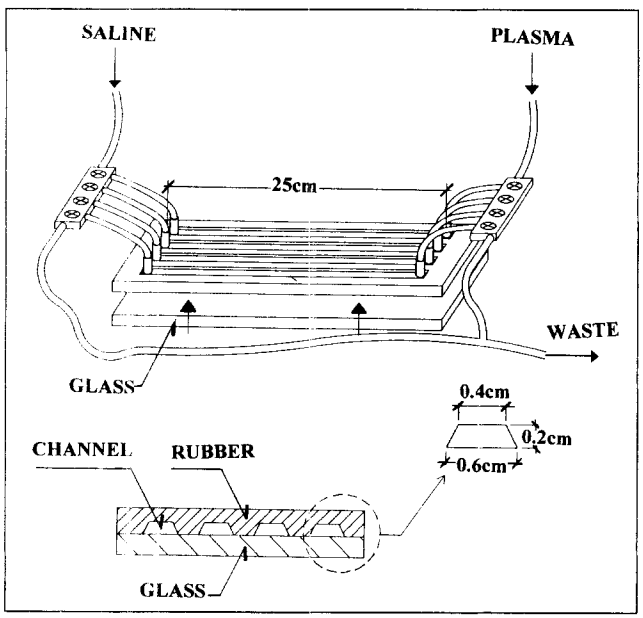

Figure 1. Shear flow chamber.

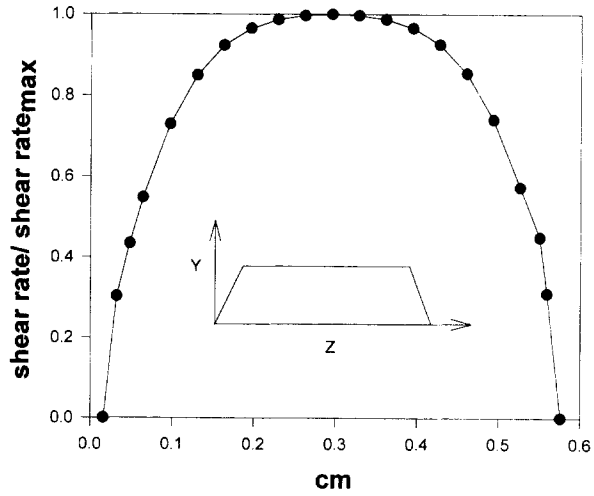

Figure 2. Shear rate distributions at the base ($y=0$) of the trapezoidal channel.

Calculated shear-rate distribution on the bottom surface of the trapezoidal channel is shown in Figure 2. It was determined by differentiating the parabola, which was fitted to the numerically calculated velocity profile at the channel's lower boundary, with respect to y. The velocity profile for fully developed laminar flow in the trapezoidal channel was solved numerically, applying a finite difference method to the following governing differential equation:

$$\frac{\partial^2 v}{\partial z^2}+\frac{\partial^2 v}{\partial y^2}=\frac{1}{\mu}\frac{dp}{dx}=\text{constant}. \qquad (1)$$

The value for the maximum velocity thus obtained is within 1.3% of that calculated by Shah (1975). Based on Shah's work, the entrance length for the channel is 0.15 cm at the maximum shear rate used. The calculated maximum velocity underestimates the maximum velocity measured by dye injection by 5.6%.

The experimental chamber was designed to assure that (a) mass transfer occurred only from parts of the flow stream in which the velocity profile was linear, and (b) the surface shear rate and velocity profile were uniform over a central region of the channel width. With respect to the first criterion, the thickness of the mass-transfer boundary layer at the end of the channel for steady-state transfer to a surface of infinite capacity was calculated. The values were 0.0078 and 0.0168 cm for shear rates of 95 s^{-1} and 9.5 s^{-1}. These values lie in a region of the total channel thickness (0.2 cm), where the axial velocity is not less than 90% of the value calculated from the wall shear rate. With respect to the second criterion, Figure 2 shows the blunted region of the shear-rate profile to be located in the central 0.2 cm of the channel.

Methods. Undiluted plasma is delivered into the saline-filled channel at a shear rate of 9.5 s^{-1}, starting at "time zero." In experiments where plasma is diluted to 30% with saline, it is delivered into the channel at a shear rate of 95 s^{-1}. Experiments are terminated by stopping the forward flow

of plasma and commencing a reverse flow with saline at 40 mL/min for 2 min (equivalent to 32 channel volumes).

After the reverse flush with saline, the glass surface is stained *in situ* (without disassembling the flow chamber) for the presence of either Fg or HMK. First, a blocking solution, containing albumin, is injected into the channel to assure that no surface remains uncovered by protein. The channel is incubated with the blocking solution for 30 min; it is then rinsed with saline and incubated in a primary antibody solution, specific to the protein of interest, for 30 min. After rinsing with saline, the chamber is incubated for 30 min with beads coated with the secondary antibody and is rinsed again with water. The chamber is then disassembled under water to prevent any disruption of the adsorbed layer of beads that might be caused by an air–water interface. The glass plate is air-dried.

The stain created by the beads is transferred to white paper with Scotch brand transparent tape. The tape–bead–paper sandwich is electronically scanned to quantify the stain intensity, as described previously (Mandrusov et al., 1996a). The protein replacement process occurring on the lower, glass surface of the channel is thus traced along the length of the channel, averaging the intensity across the central 0.2 cm of the channel where the shear-rate profile is blunted. The intensity of the stain correlates quantitatively with the amount of specific protein adsorbed out of the protein solution (darker stain implying more protein present). The intensity reading (I) varies between 0 (lightest) and 0.25 (darkest), measured in arbitrary units. The negative control for the assay was obtained by exposure of a virgin surface (one that has not seen blood plasma) to the bead immunoassay. The controls produced an average reading of 0.06. Thus, readings up to 0.06 units were interpreted as background and the assay sensitivity threshold is set at $I = 0.06$.

The bead immunoassay saturates at concentrations lower than those needed to cover the surface with protein. Saturation is a consequence of the design of the assay: antibody loading on the particles was optimized to give high sensitivity to the target adsorbate. Thus a monolayer of beads can form on a surface that is only fractionally covered with the adsorbed protein of interest. By comparison of the published Fg isotherm data (bulk concentration [mg/mL] vs. surface coverage [$\mu g/cm^2$]) (Cornellius et al., 1992) and the Fg isotherm obtained with the bead data (bulk concentration [mg/mL] vs. stain intensity [I]) (Mandrusov et al., 1996a), it is inferred that a monolayer of beads ($I = 0.25$) corresponds to 0.03 $\mu g/cm^2$ of Fg. The lowest detectable amount ($I = 0.06$) of Fg corresponds to 0.0003 $\mu g/cm^2$ (effectively zero concentration). Since there is no published HMK isotherm, interpretations of adsorption patterns can only be qualitative.

In order to show that adsorbed Fg is capable of participating in the thrombotic process, glass surfaces were exposed to platelets. The glass plates, removed from the shear-flow chamber, were blocked with BSA for 30 min, incubated in the platelet suspension (in Tyrode's buffer) in the staining well for 30 min at room temperature, then were gently washed with normal saline, and then were fixed in 1% paraformaldehyde. The fixed slides were stained with the Coomassie blue dye, and the number of adherent platelets was counted using an upright Olympus BH-2 microscope with an attached video camera. The platelets were counted along the length of the channel. At each position three points (at the center of the channel and 0.5 mm away from the center of either side) were counted and averaged, using field of view 0.08×0.08 mm. Error bars on the figures represent standard deviations for each axial position.

Experimental Results

The rate of protein deposition on the surface greatly depends on the degree of plasma dilution and the shear rate of the flow. Using high plasma concentrations in conjunction with high shear rates produces transients too fast to analyze in this system. Thus, the experimental results presented here are divided into two sets: (1) 30% plasma at a high shear rate (95 s^{-1}), and (2) 100% plasma at a low shear rate (9.5 s^{-1}). In the first set, deposition of both fibrinogen and HMK is studied. In the second set Fg deposition is studied and is shown to mediate platelet adhesion to the surface. The Fg wave width is measured at half maximum height above the intensity threshold ($I = 0.06$) and the wave velocity is measured at half-width (at half maximum height).

Protein deposition out of 30% plasma at 95 s^{-1}

Figure 3 illustrates the distribution of Fg and HMK on the glass surface along the length of the channel at several times: Figure 3a shows the distribution of the two proteins at 12 s after plasma injection; Figures 3b, 3c and 3d show the distribution after 22, 67 and 127 s, respectively. The horizontal line indicates where the intensity readings fall below the sensitivity threshold of the assay. After 12 s, both Fg and HMK are deposited along the surface, with Fg leading HMK by about 10 cm. After 22 s assay-saturating amounts of Fg are observed throughout the channel and HMK deposition is at saturating levels up to 7 cm away from the entrance to the channel. After 67 s, Fg replacement is seen up to 4 cm away from the entrance to the channel, and HMK deposition is at saturating levels up to 15 cm away from the entrance to the channel. After 127 s, the channel is devoid of Fg and saturating amounts of HMK are present throughout the channel. At this shear rate the full Fg–HMK profile cannot be captured on the bottom surface of the 25-cm length of channel.

Protein deposition out of 100% plasma at 9.5 s^{-1}

The entire Fg–HMK profile could be captured in the 25-cm-long channel using whole plasma injected at a shear rate of 9.5 s^{-1}. Figure 4 shows the distribution of Fg along the length of the channel at four successive time points: 37, 52, 67, and 82 s after plasma injection. The horizontal line indicates where the intensity readings fall below the sensitivity threshold of the assay. The Fg wave appears to travel at an increasing speed: 0.17 cm/s after 37 s and 0.25 cm/s after 82 s (using half-width at half-height of each wave as a measuring point). The average width of the wave, measured at half maximum intensity above the threshold for each wave, is 3.3 cm.

Platelet adhesion to surfaces exposed to plasma at shear rate of 9.5 s^{-1}

A comparison between Fg deposition and platelet adhesion, subsequent to exposure of the prewetted glass surfaces to undiluted plasma at 37, 52 67 and 82 s after plasma injec-

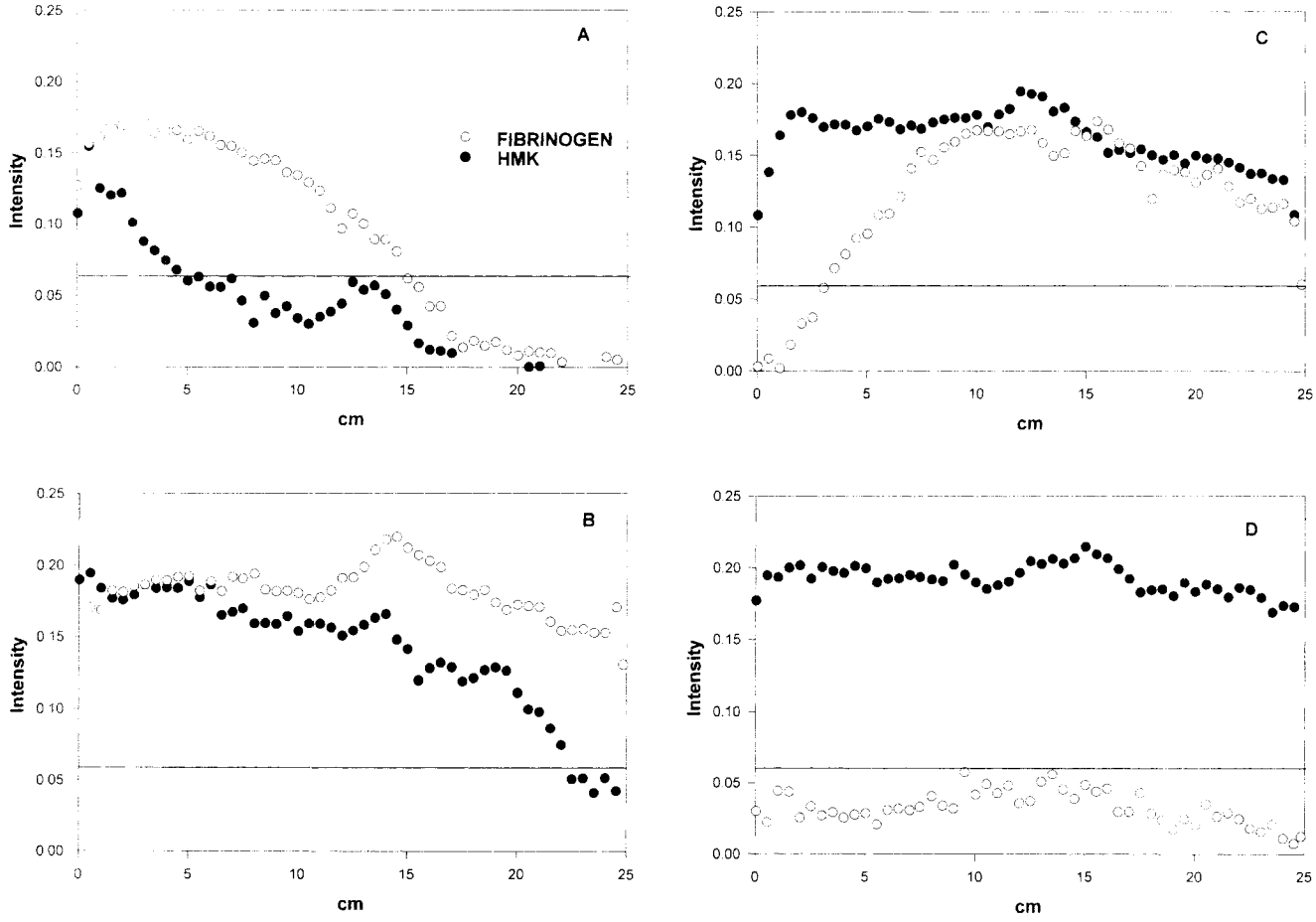

Figure 3. Protein adsorption to glass out of 30% plasma at 95 s^{-1}: (○) fibrinogen and (●) HMK.

Times of exposure are 12 s (a), 22 s (b), 67 s (c), and 127 s (d). Each curve represents an average of 5 separate experiments ($N = 5$), average standard deviation is ± 0.03. Error bars are omitted for clarity. The horizontal line indicates where intensity is below the sensitivity threshold of the assay.

tion at the shear rate of 9.5 s^{-1}, is shown in Figures 5a, 5b, 5c and 5d, respectively. The vertical scales are adjusted to render platelet and Fg peaks comparable. In all of the panels, platelets appear to adhere where Fg is present. The wave width (measured at half-height) increases with time: 2.5 cm after 37 s and 3.5 cm after 82 s. The platelet adhesion wave also travels at an increasing speed: 0.19 cm/s after 37 s and 0.27 cm/s after 82 s (using half-width at half-height of each wave as a measuring point). Morphologically, platelets appear maximally spread when they are at their highest density (on the average 12.5×10^4 cells/mm^2). At this density frequent aggregates consisting of 10–15 cells are observed.

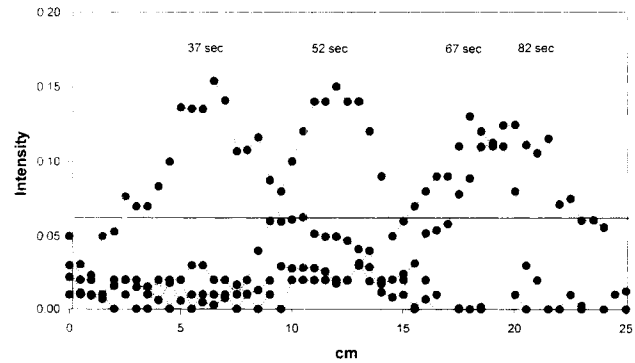

Figure 4. Fibrinogen adsorption to glass out of 100% plasma at 9.5 s^{-1}.

$N = 5$, average standard deviation is ± 0.02. Error bars are omitted for clarity. The horizontal line indicates where intensity is below the sensitivity threshold of the assay.

Simple Kinetic Model of the Vroman Effect

This section is divided into four short parts. The first presents a simple kinetic model of the Vroman effect. The second extends the classic Leveque solution to the unsteady-state convective diffusion problem with nonlinear (saturating) boundary conditions. The third describes the numerical approach used for solving the Leveque problem. The fourth presents the model predictions for 30% and 100% plasma.

Overview of the model

The overall Vroman effect can be modeled as a multicomponent transient convective-diffusion problem, within a steady duct flow, with no reactions among species in the bulk, and with boundary conditions that take into the account the in-

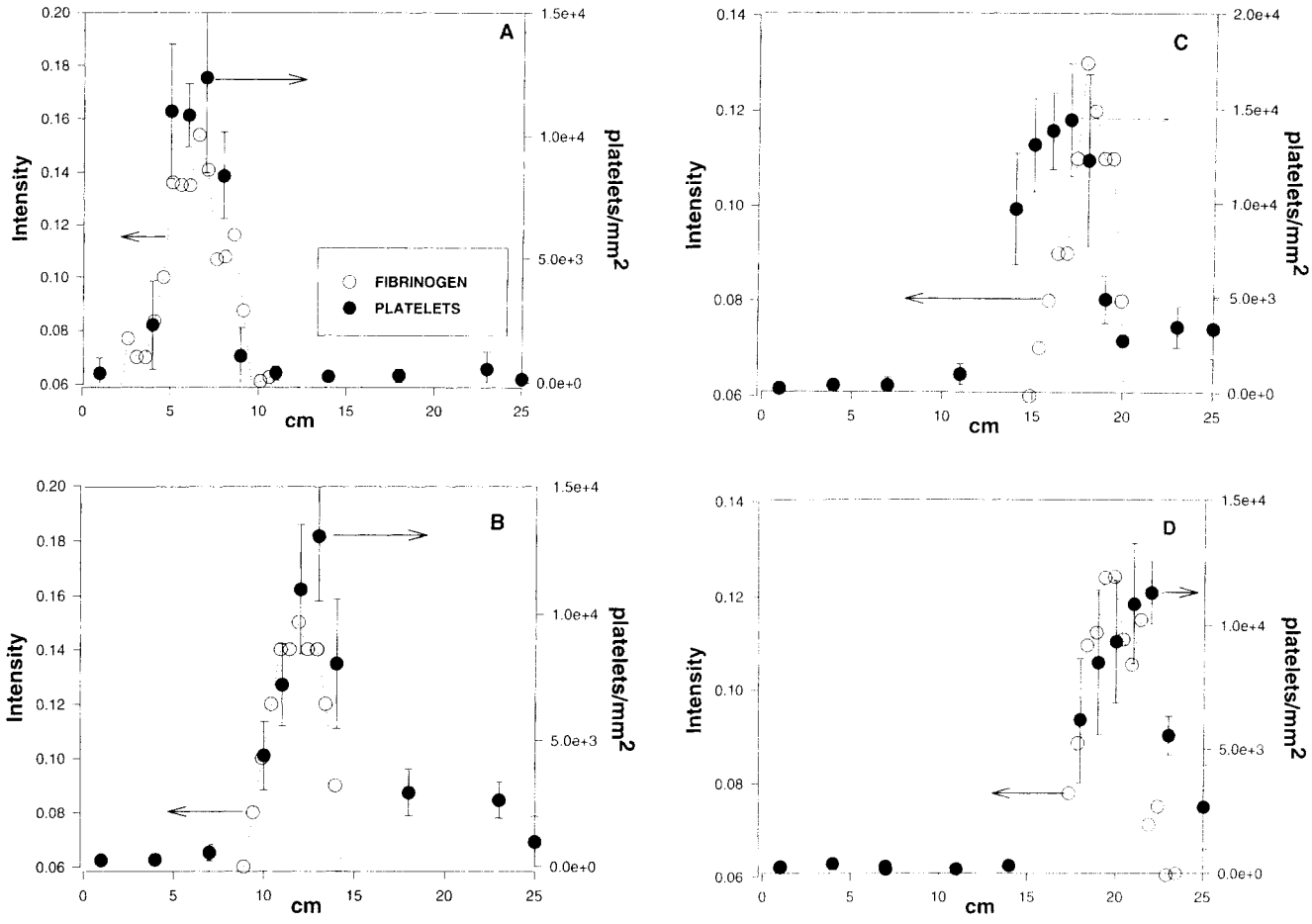

Figure 5. Fibrinogen adsorption and platelet adhesion to glass exposed to 100% plasma at 9.5 s^{-1}: (○) fibrinogen ($N = 5$) and (●) platelets ($N = 3$).

Times of exposure are 37 s (a), 52 s (b), 67 s (c), and 82 s (d). The vertical scales were adjusted to make the platelet and Fg peak heights comparable.

teractions among the proteins on the surface. The simple model presented here considers only interactions between the two key plasma proteins. It is assumed that Fg instantaneously displaces any protein that had previously adsorbed (the kinetics of albumin and IgG are not considered) and that HMK instantly displaces Fg:

$$\mathrm{Fg}|_S = \int_0^t N_{\mathrm{Fg}}|_S \, d\tau - \int_0^t N_{\mathrm{HMK}}|_S \, d\tau;$$

$$\mathrm{HMK}|_S = \int_0^t N_{\mathrm{HMK}}|_S \, d\tau. \quad (2)$$

Because of the higher concentration of Fg, its deposition is essentially unaffected by HMK, which adsorbs later. Because HMK is assumed to displace Fg instantaneously, its pattern of deposition is unaffected by how much Fg is on the surface. Thus, deposition of the two proteins can be regarded as two independent events and the net amount of Fg (deposition minus replacement) is the difference between deposition of Fg and of HMK. This model requires, then, only the calculation of two independent depositions—one for Fg and the other for HMK—with which the Fg profile is calculated afterward as their difference.

Transient Leveque problem

Figure 6 shows the domain of the problem. The y-coordinate originates on and is normal to the adsorbing surface. The x-coordinate originates at the beginning of the channel. Height H corresponds to the steady-state mass-transfer boundary-layer thickness calculated at the end of the channel. This value in all cases is less than 10% of the experimental channel height. The channel length is L. The velocity profile is taken to be linear, its slope equal to the wall shear rate.

A single-component unsteady convective-diffusion equation:

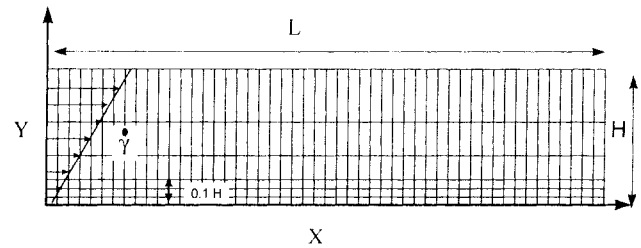

Figure 6. Problem domain.

$$\frac{\partial c_i}{\partial t} = D_i \frac{\partial^2 c_i}{\partial y^2} - y\dot{\gamma}\frac{\partial c_i}{\partial x} \tag{3}$$

may be used to describe the kinetics of deposition of a single protein out of a fluid that has a linear velocity profile, $v_x = \dot{\gamma} y$ ($\dot{\gamma}$ is the shear rate at the wall). It is assumed that the adsorbed protein does not diminish capacity of the wall to adsorb (i.e., concentration is always zero at the adsorbing surface) until the wall is saturated and the flux of the given protein is set to zero.

The boundary conditions are

$C_i = C_{io}$ as $y = H$

$C_i = 0$ at $y = 0$ if the surface capacity for protein has not been reached

$\frac{dc_i}{dy} = 0$ at $y = 0$ otherwise.

The entrance condition is

$$C_i = C_{io} \quad \text{at} \quad x = 0.$$

The initial condition is

$$C_i = 0 \quad \text{at} \quad t = 0.$$

Numerical solution

Governing Equation. In Eq. 3, the x-directed diffusion term is neglected since it is much smaller than the x-directed convection. However, in the numeric formulation, the x-directed diffusion term is reinserted and the equation is nondimensionalized:

$$D_i^* \frac{\partial^2 c_i^*}{\partial y^{*2}} + D_i^* \frac{\partial^2 c_i^*}{\partial x^{*2}} = \frac{\partial c_i^*}{\partial t^*} + y^* Pe \frac{\partial c_i^*}{\partial x^*}, \tag{4}$$

where

$$t^* = \frac{D_1}{L^2} t, \quad c_i^* = \frac{C_i}{C_o}, \quad x^* = \frac{x}{L},$$

$$y^* = \frac{y}{L}, \quad D_i^* = \frac{D_i}{D_1} \quad \text{and} \quad Pe = \frac{\dot{\gamma} L^2}{D_1}.$$

The nondimensional boundary conditions are

$C_i^* = 0$ at $y^* = 0$ if the surface capacity for protein has not been reached

$\frac{dc_i^*}{dy^*} = 0$ at $y^* = 0$ otherwise.

The surface coverage at any point along the adsorbing wall is calculated by summing the flux at that point from 0 to t (see Eq. 2):

$$\Gamma^* = \sum \frac{dc_i^*}{dy^*} \Delta t^*.$$

The maximum surface capacity is given by

$$\Gamma_{\max}^* = \frac{\Gamma_{\max}}{C_0 L}.$$

The free-stream boundary condition becomes

$$C_i^* = 1 \quad \text{at} \quad y^* = 1,$$

with the entrance condition:

$$C_i^* = 1 \quad \text{at} \quad x^* = 0$$

and the initial condition:

$$C_i^* = 0 \quad \text{at} \quad t^* = 0.$$

These boundary conditions, along with Eq. 4, are implemented in the computer code.

Validation of the Numerical Code. A finite volume method (FVM), which utilizes the discretized form of the conservation equations, and an upwind scheme for interpolation of the concentration profiles, valid for high Pe number flows (Patankar, 1980), was applied to the governing equation. The problem domain contains 450×50 rectangular grids, as shown in Figure 6. The grid is uniform in the x-direction. In the y-direction, the grid is nonuniform, with higher grid density near the adsorbing surface. The iterations in time are completed with a fixed time step of 4.32×10^{-12} dimensionless time units. Numerical experiments showed that increasing the grid density beyond 450×50 or decreasing the time step did not change the solution. The concentration profile at any x, along the y-direction, showed significant concentration gradients at $y^* \ll 1$. Numerical results, obtained by allowing the transient solution to run until no variations in concentration with respect to time were observed, matched the analytical Leveque solution within 1% for $x^* > 0.09$ (Yang, 1997).

Model predictions

Simulation inputs. Numerical simulations of both Fg and HMK transient adsorption were conducted for the two cases that correspond to the experiments described earlier: (1) 30% plasma at 95 s^{-1}, and (2) 100% plasma at 9.5 s^{-1}. Table 1 summarizes the physical constants used to parameterize the simulation.

Data Presentation. The model predictions are given over the full range of possible surface concentrations (from 0.00 to 0.35 $\mu g/cm^2$). However, the calculations are compared with measurements only over the range of the assay—between the surface concentration at which the assay saturates, 0.03 $\mu g/cm^2$, and the lowest detectable amount, 0.003 $\mu g/cm^2$. So that the values in the assay range can be read more clearly, the insets in the graphs show the same result on a semilogarithmic scale. The Fg wave width is measured at half-height value for the assay saturation ($\Gamma = 0.015$ $\mu g/cm^2$), and the wave velocity is measured at half-width (at half saturation height).

Table 1. Physical Constants Used in the Computer Model

Parameter		Literature Source
Diffusivity	$D_{Fg} = 2\times10^{-7}$ cm^2/s	Andrade and Hlade (1987)
	$D_{HMK} = 1.46\ D_{Fg}$	*See below
Molecular wt.	Fg = 340,000 g/mo	Andrade and Hlade (1987)
	HMK = 110,000 g/mo	Dejardin et al. (1995)
Human blood plasma conc.	Fg = 3 mg/mL	Dejardin et al. (1995)
	HMK = 0.070 mg/mL	Dejardin et al. (1995)
Max. surface coverage based on side-on packing	Fg = 0.2 μg/mL	Yan and Dejardin (1991)
	HMK = 0.35 μg/mL	Dejardin et al. (1995)

*HMK diffusivity is taken to be proportional to the cube root of the ratio of the molecular weights of Fg to HMK.

Protein Deposition out of 30% Plasma at 95 s^{-1}. Figures 7a and 7b present model predictions for the distribution of Fg and HMK on the surface of the glass. Figure 7a shows Fg movement after surface exposure to flowing 30% plasma. After 12 s, the detectable Fg wavefront has moved 5 cm into the channel. After 22 s, it traveled 15 cm and the wave velocity (measured at half-width) increased from 0.10 cm/s to 0.27 cm/s. The wave width is doubled in comparison to that at 12 s. After 67 s, the leading edge of the Fg wave is no longer observable in the channel. At this time the model predicts that most of the channel surface is covered with Fg. After 127 s, the replacement of Fg by HMK is completed 3 cm away from the entrance to the channel. Figure 7b shows HMK deposition along the length of the channel. The leading edge of deposition of HMK slightly trails behind that of Fg after 12 and 22 s. After 67 and 127 s, the amounts of protein are saturating with respect to the assay throughout the channel.

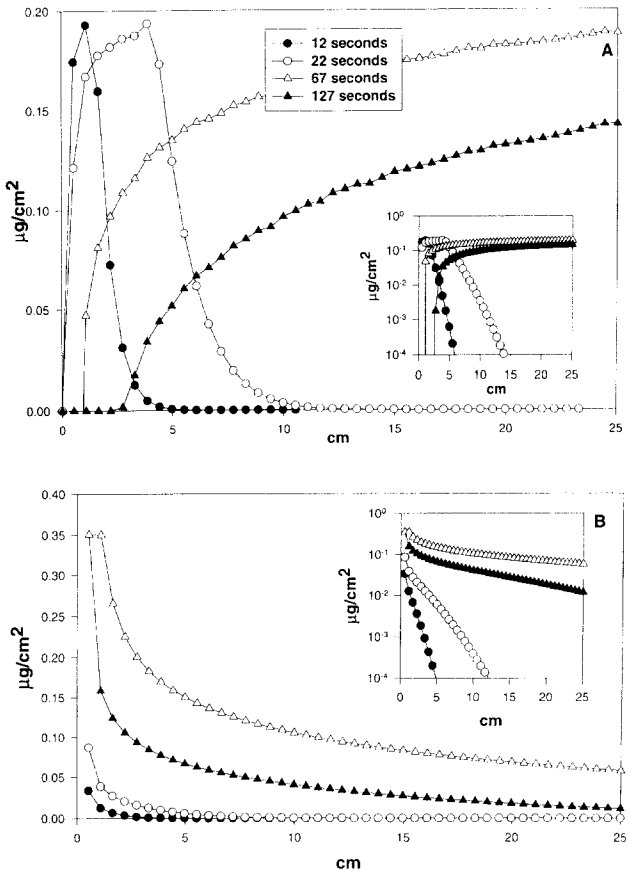

Figure 7. Model prediction for the protein adsorption to glass exposed to 30% plasma at 95 s^{-1}.

(a) Fibrinogen and (b) HMK. Times of exposure are 12 s (●), 22 s (○), 67 s (▲), and 127 s (△). The insert shows the same data on the semilog scale.

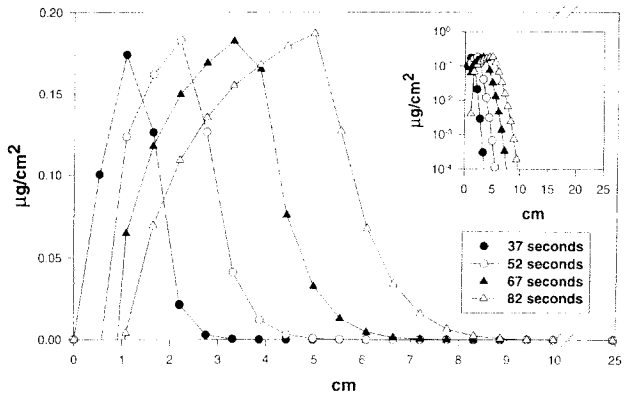

Figure 8. Model prediction for the Fg adsorption to glass exposed to 100% plasma at 9.5 s^{-1}.

Times of exposure are 37 s (●), 52 s (○), 67 s (▲), and 82 s (△). The insert shows the same data on the semilog scale.

Protein Deposition out of 100% Plasma at 9.5 s^{-1}. Figure 8 presents the predicted movement of Fg when glass is exposed to undiluted flowing plasma. The model shows that the wave width increases with time for all time points studied. The velocity of the wave (measured at half-width) also increases with time: 0.045 cm/s after 37 s and 0.067 cm/s after 82 s of exposure.

Discussion

The data presented in the preceding establish the existence of a wave of Fg that moves along the boundary of a shear flow of blood plasma. At the lower shear rate (9.5 s^{-1}), the entire Fg wave, front to back, is revealed as it sweeps along the surface of the 25-cm-long channel. This wave is defined at its front by the leading edge of Fg deposition and at its back by the region where Fg is removed by HMK. Displacement of Fg by other plasma proteins is similar to phenomena encountered in displacement chromatography (King, 1980), except that the entire process, adsorption and displacement, takes place under one solution—the feed is not switched from a loading to displacing solution. At the higher shear rate (95 s^{-1}), the wave width is larger than the channel length, and the proteins coexist during the initial times of exposure, with Fg eventually appearing to be replaced by HMK. Focusing on a single surface point, one sees the amount of Fg on the surface rising through a maximum and then eventually disappearing. For instance, at $x = 20$ cm, the amount of Fg on the surface increases from 0 to 0.17 intensity units after 22 s and then drops down to 0.14 after 67 s. It disappears by 127 s. This behavior is a classic example of the Vroman effect (Vroman and Adams, 1986; Vroman and Leonard, 1991; Wojciechowski et al., 1986; Slack et al., 1991).

Suspended, resting platelets, which settle on the surfaces exposed to plasma, adhere only to places where Fg is present. It is of interest to note that while surface-bound Fg has been implicated in mediating platelet adhesion, surface-bound HMK has been shown to possess the strongest antiadhesive effect when adsorbed onto otherwise adhesive surfaces (Asakura et al., 1992). Adhesion of resting platelets to surface-bound Fg is mediated through the platelets' glycoprotein IIb subunit (Savage and Ruggeri, 1991; Savage et al., 1992). Rye et al. (1995) have demonstrated that only conformationally intact (antibody detectable) Fg bound to a surface can be correlated with platelet activity. This is also in accord with data of Chinn et al. (1991), who have exposed platelet suspensions to polyurethane surfaces (Biomer), that were previously exposed to plasma under static and shearing conditions; in both cases the largest number of adhered platelets correlated with the largest amounts of Fg present on the surface. Mandrusov et al. (1996b) have also reported correspondence between Fg adsorption and platelet adhesion on glass slides that have been previously exposed to plasma in regions of separated flow.

While the calculated transients mimic the experiments, the model underestimated both the width and the velocity of the wave. Since the total wave was only captured with 100% plasma, the comparisons between the experimental results and numerical predictions for the wave width and wave velocity can be presented for this case; the comparisons for the leading edge of deposition are presented for both 30% and 100% plasma. Table 2 compares experimental results to the model prediction. After 37 s of exposure of glass to the undiluted plasma supplied at 9.5 s^{-1}, the predicted velocity was 0.045 cm/s and the measured velocity was 0.17 cm/s. At this time, the predicted width of 3.0 cm was close to the measured width of 3.3 cm. However, after 82 s the discrepancy between the predicted and the measured wave width increased: the predicted was 8 cm and the measured 3.9 cm. For all times studied the velocity of the wave is about four times larger than that predicted by the model. The leading edges of Fg deposition for both 100% and 30% plasma cases exceeded the model predictions, with larger discrepancy for the 100% plasma than for the 30% plasma studies (in terms of the ratios experimental results/model predictions).

In response to this disparity, model parameters have been varied to see if faster rates of deposition might be predicted. Decreasing the surface capacity or increasing protein concentration (within physiological limits) did not result in significant increase in the rate of Fg deposition. It might be argued that the proposed model is too simple and should incorporate in it other surface-active proteins participating in the Vroman effect, finite adsorption, as well as different adsorption states for these proteins. But these modifications would only delay, rather than accelerate the predicted rates of deposition of Fg.

A possible cause of the discrepancy between model and the experiment is the presence of natural convection in the system, arising from the density differences between the injected fluid (undiluted plasma (1.0273 g/cm^3), 30% plasma (1.0082 g/cm^3) (Altman, 1961)) and the prefilled saline it displaces (1.000 g/cm^3). If plasma, which is heavier than saline, sinks down as it enters the channel, then the mass-transfer boundary-layer thickness becomes smaller at the bottom surface and larger at the upper surface, increasing protein transport to the bottom surface and decreasing it to the top. In order to investigate whether this is the case, two additional experiments were completed at 9.5 s^{-1}: (1) an undiluted plasma was supplied to the channel with the adsorbing surface located above the stream, and (2) a pure Fg solution (3-mg/mL Fg, in normal saline) was injected into the channel with the adsorbing surface located below the stream (this solution has a density very close to that of saline). The Fg deposition patterns were measured in both cases and compared to the already reported case of an undiluted plasma injected into the channel with the adsorbing surface located below the stream. The results, presented in Figure 9, indicate that after 67 s of exposure, the Fg wave moved 5 cm on the upper surface, whereas it moved 21 cm on the lower surface. A pure Fg solution adsorbed along 7.2 cm of the channel surface. The movement of Fg on the upper surface lagged the computer prediction by 5 cm, while that movement on the lower surface led the prediction by 10 cm. The adsorption of Fg along the channel surface out of pure Fg solution, where there

Table 2. Comparison Between Experimental Results and Model Prediction*

Time (s)	100% Fg Wave Width (cm)	100% Fg Wave Vel. (cm/s)	100% Fg Leading Edge of Deposition (cm/s)	30% Fg Leading Edge of Deposition (cm/s)
37	3.3/3.0	0.17/0.045	9.5/3.2	15.0/6.0
52	3.7/4.6	0.24/0.056	14.5/5.2	23.0/14.0
67	2.4/6.2	0.28/0.061	20.2/7.2	Not observed
82	3.9/8.0	0.25/0.067	23.0/9.2	Not observed

*Each table entry shows experimental/predicted value.

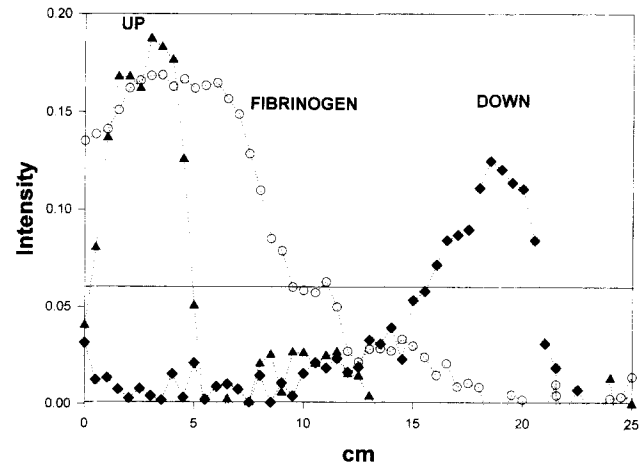

Figure 9. Fibrinogen adsorption to the upper surface of the channel out of 100% plasma at 9.5 s^{-1} (UP, ▲), to the lower surface of the channel out of 100% plasma (DOWN, ♦) $N = 5$, average standard deviation ± 0.02, and to the lower surface of the channel out pure Fg solution at concentration 3 mg/mL in normal saline (○), $N = 4$, average standard deviation ± 0.02.

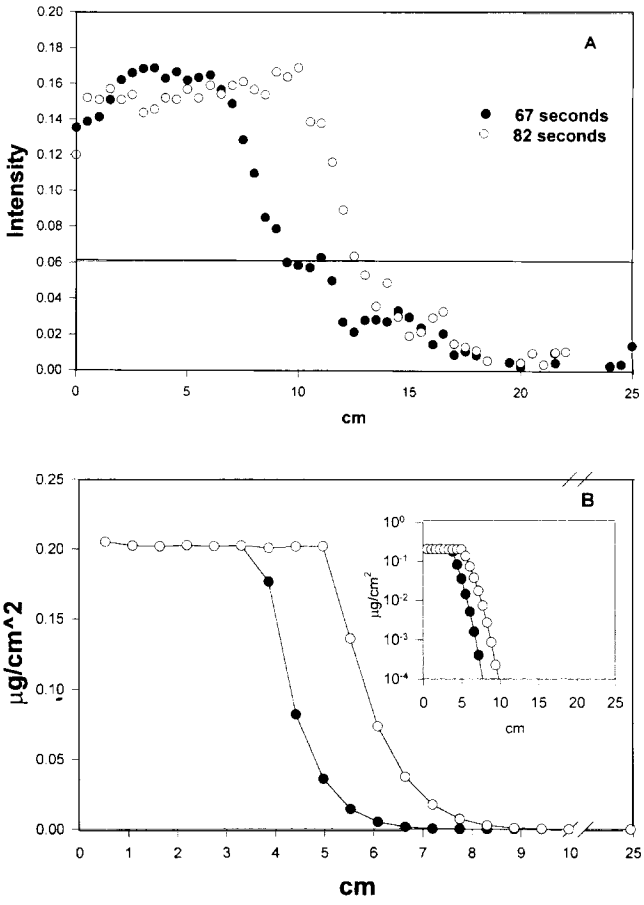

Figure 10. Comparison between the model prediction for the Fg adsorption to glass exposed to the Fg solution (3 mg/mL) at 9.5 s^{-1}.

(a) Experimental data for Fg deposition after 67 s (●) and 82 s (○), $N = 4$, average standard deviation ± 0.02. Error bars are omitted for clarity. The horizontal line indicates where intensity is below the sensitivity threshold of the assay. (b) Model prediction for Fg deposition after 67 s (●) and 82 s (○). The inset shows the same data on the semilogarithmic scale.

are no density differences between the injected fluid and the preexisting fluid, approximated the prediction of the model, which does not take into account the natural convection effects (Figures 10a and 10b). Thus, these data strongly suggest that the natural convection plays an important role in protein deposition out of whole plasma—the density difference accelerates the transport of proteins toward the adsorbing surface if it is located below the stream and retards the transport if the adsorbing surface is located above the stream. Although the pure Fg studies show a good correspondence between the predicted and experimental results, these studies were not further investigated because the purpose of this work was to demonstrate and analyze the Vroman effect (plasma protein surface reactions), relevant to the development of thrombosis in artificial organs. Furthermore, density differences due to variations in temperature and concentration could not be avoided in actual clinical practice and will affect deposition in different ways, as could also the orientation of the device.

A description of the phenomena of natural convection caused by density difference between the injected and prefilled fluids is represented in Figure 11. At short times, the pure convection tends to prevail, and this creates a parabolic finger of the injected plasma, which grows out into the channel so that the maximum protein concentration is at the center of the channel. The action of gravity tends to make material at the core sink to the bottom of the channel, thereby causing the displaced fluid layers to circulate. In this sense natural convection increases radial mixing, and the sinking of the core creates a smaller mass-transfer boundary layer thickness at the bottom surface, and a bigger one on the top surface.

No prior studies have been found that deal directly with the effects of natural convection, caused by the density differences between the displacing and the displaced fluids, on the protein transport to the surface. Reejhsinhani et al. (1966) have studied the effects of free convection on the dispersion of dye in the water prefilled channel. They have reported that the natural convection can both enhance and depress dispersion significantly and that extremely small density differences ($\Delta\rho/\rho = 10^{-4}$) are adequate to cause these phenomena. Most other works deal with free convection, where the density differences in the fluid are induced by the heating or cooling of the walls of the conduit into which the fluid is injected, producing a circulatory motion of the fluid in the direction normal to pipe axes, in so-called secondary flow (Gebhart et al., 1988). This situation is different from the present work, since the density differences reported here are not induced, but preexisting.

Due to the lack of analysis of the relative importance of the natural convection in the situation reported in this work, this assessment is completed for the heat-transfer systems. The demarcation between the purely forced and the combined (as well as purely natural and combined) regimes is given in terms of the dimensionless group Grashof number/(Reynolds number)^2 (Gebhart et al., 1988). The Grashof (Gr) number and the Reynolds number (Re) are defined as

$$Gr = \frac{g\Delta\rho D_h^3}{\rho\upsilon^2} \quad \text{and} \quad Re = \frac{VD_h}{\upsilon^2},$$

where D_h is the hydraulic diameter of the channel (area/pe-

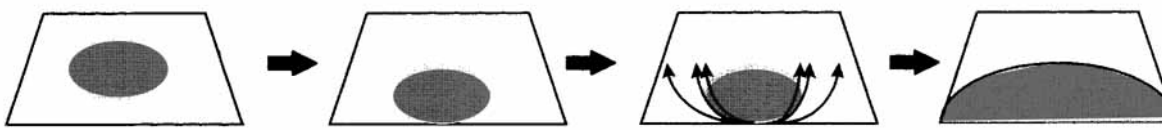

Figure 11. Natural convection caused by density difference between the injected and prefilled fluids.

The action of gravity tends to make material at the core sink to the bottom of the channel, thereby causing circulation of the displaced fluid layers.

Table 3. Values for the Two Tested Experimental Systems

	Re	Gr	Gr/Re^2
100% plasma at 9.5 s^{-1}	1.6	91.2	35.2
Of 30% plasma at 95 s^{-1}	16.1	27.9	0.1

rimeter). Table 3 summarizes the values for the two experimental systems tested. The values of Gr/Re^2 indicate the existence of the natural convection for the experiments completed with 100% plasma. For 30% plasma experiments, the natural convection appears to be less evident. This information supports the reported findings: there is less discrepancy between the model and the experiments in the 30% plasma than in the 100% plasma, and even less if pure Fg solution is injected into the channel.

What do the results just presented suggest about the possible causes of thrombosis on prewetted clinical devices? For the first time unequivocal evidence is presented that an Fg band forms and that even quiescent platelets stick to it. Thus, there is a temporal and spatial window during the device startup when Fg is present on the surface and is able to bind and activate platelets and initiate thrombosis. The presence of traveling Fg bands is consistent with well-documented theories of protein replacement and is in general accord with a simple model that focuses on Fg, the central protein in thrombogenesis. The velocity of the Fg band, traveling along surfaces when the device is first filled with blood, increases due to the free convection if the adsorbing surface is located on the bottom and decreases if it is located on the top. The width of the Fg band increases as the wave progresses into the channel. However, as the wave travels, it continues to widen and may reach a critical width at which either the amount or conformation of Fg is no longer adequate to induce platelet binding. Thus, the chances that thrombi and emboli will form may be especially great near the entrance to the channel, immediately after the device is first exposed to blood.

Acknowledgments

This work was supported by the National Institutes of Health Grant HL-44535 and by contributors to the Artificial Organs Research Fund at Columbia University.

Notation

C = concentration, mg/mL
C_0 = input concentration, mg/mL
D = diffusion coefficient, cm^2/s
L = length of the channel, cm
t = time, s
t_{ss} = time to reach steady state, s
N = flux, $\mu g/(cm^2 \cdot s)$
Pe = Peclet number
x, y = Cartesian coordinates
v_x = velocity in x-direction, cm/s
Γ = surface capacity, $\mu g/cm^2$
δ = mass-transfer boundary-layer thickness, cm
υ = kinematic viscosity, cm^2/s
τ = time
$\dot{\gamma}$ = shear rate, s^{-1}

Subscripts and superscripts

I = belonging to the ith specie
$*$ = dimensionless variable

Literature Cited

Altman, P. L., "Blood and Other Body Fluids," Federation of American Society for Experimental Biology, Washington, DC (1961).
Andrade, J. D., and V. Hlady, "Plasma Protein Adsorption: The Big Twelve," *Ann. NY Acad. Sci.*, **516**, 158 (1987).
Asakura, S., R. W. Hurley, K. Skorstengaard, I. Okhubo, and D. F. Mosher, "Inhibition of Cell Adhesion by High Molecular Weight Kininogen," *J. Cell Biol.*, **116**, 465 (1992).
Bouzama, A., P. Dejardin, F. Y. Bauduin, and Y. Holl, "Fibrinogen Adsorption on Pyrex Glass Tubes: A Continuous Kinetic Study," *Biophys. Chem.*, **42**, 87 (1992).
Chinn, J. A., T. A. Horbett, and B. D. Ratner, "Baboon Fibrinogen Adsorption and Platelet Adhesion to Polymeric Materials," *Thromb. Haemostasis.*, **65**, 608 (1991).
Cornellius, R. M., P. Wojciechowski, and J. L. Brash, "Measurement of Protein Adsorption Kinetics by In-situ, 'Real-Time,' Solution Depletion Techniques," *J. Colloid Interf. Sci.*, **150**, 121 (1992).
Dejardin, P., "Coupling Between Bulk Diffusion/Convection and Interfacial Adsorption/Desorption: The Linear Gradient Approximation with Langmuir Excluded Surface Effect," *J. Colloid Interf. Sci.*, **133**, 418 (1989).
Dejardin, P., P. ten Hove, X. J. Yu, and J. L. Brash, "Competitive Adsorption of High Molecular Weight Kininogen and Fibrinogen from Binary Mixture to Glass Surface," *Langmuir*, **11**, 4001 (1995).
Gebhart, B., Y. Jaluria, R. L. Manajan, and B. Sammaki, *Buoyancy Induced Flows and Transport*, Hemisphere, New York (1988).
King, C. J., *Separation Processes*, McGraw-Hill, New York (1980).
LeDuc, C. A., N. DePaola, S. Konath, L. Vroman, and E. F. Leonard, "Adsorption of Proteins out of Plasma Onto Glass from Separated Flow," *J. Biomater. Sci. Poly. Ed.*, **6**, 599 (1994).
LeDuc, C. A., L. Vroman, and E. F. Leonard, "A Mathematical Model for the Vroman Effect," *Ind. Eng. Chem. Res.*, **34**, 3488 (1995).
Lu, C. F., A. Nadarajah, and K. K. Chittur, "A Comprehensive Model for Multiprotein Adsorption on Surfaces," *J. Colloid Interf. Sci.*, **168**, 152 (1994).
Mandrusov, E., L. Vroman, and E. F. Leonard, "Detection of Specific Plasma Proteins on Extensive Surfaces by Immunospecific Adhesion of Dyed Polystyrene Beads," *J. Biomater. Sci. Poly. Ed.*, **8**, 1 (1996a).
Mandrusov, E., L. Vroman, E. G. Puszkin, and E. F. Leonard, "Separated Flows in Artificial Organs: A Cause for Early Thrombogenesis?," *ASAIO J. Trans.*, **42**, M506 (1996b).
Patankar, S. V., *Numerical Heat Transfer and Fluid Flow*, Taylor & Francis, London (1980).
Reejhsinghani, N. S., W. L. Gill, and A. J. Barduhn, "Experiments in Horizontal Tubes Including Observations of Natural Convection Effects," Part III, *AIChE J.*, **12**, 916 (1966).
Rye, G. H., J. Kim, Z. M. Ruggeri, S. H. Han, J. H. Kim, and B. G. Min, "Effect of Shear Stress on Fibrinogen Adsorption and Its Conformational Change," *ASAIO J. Trans.*, **41**, M384 (1995).
Savage, B., and Z. M. Ruggeri, "Selective Recognition of Adhesive Sites in Surface-Bound Fibrinogen by Glycoprotein IIb-IIIa on Nonactivated Platelets," *J. Biol. Chem.*, **266**, 11227 (1991).
Savage, B., S. J. Shatti, and Z. M. Ruggeri, "Modulation of Platelet Function Through Adhesion Receptors," *J. Biol. Chem.*, **267**, 11300 (1992).
Shah, R. K., "Laminar Flow Friction and Forced Convection Heat Transfer in Ducts of Arbitrary Geometry," *Int. J. Heat Mass Transf.*, **18**, 849 (1975).
Slack, M. S., and T. A. Horbett, "Changes in Strength of Fibrinogen Attachment on Solid Surfaces: An Explanation of the Influence of Surface Chemistry on the Vroman Effect," *J. Colloid Interf. Sci.*, **133**, 148 (1989).
Slack, M. S., and T. A. Horbett, "The Vroman Effect: A Critical Review," ACS Symp. Series, **602**, 112 (1995).
Slack, M. S., S. E. Posso, and T. A. Horbett, "Measurement of Fi-

brinogen Adsorption from Blood Plasma Using ^{125}I-Fibrinogen and a Direct ELISA Technique," *J. Biomater. Sci. Poly. Ed.*, **3**, 49 (1991).
Vroman, L., A. L. Adams, G. C. Fischer, and P. C. Mynoz, "Interaction of HMK, Factor XII, and Fibrinogen in Plasma at Interfaces," *Blood*, **55**, 156 (1980).
Vroman, L., and A. L. Adams, "Adsorption of Proteins out of Plasma and Solutions in Narrow Spaces," *J. Colloid Interf. Sci.*, **111**, 391 (1986).
Vroman, L., and E. F. Leonard, "The Effect of Flow on Displacement of Proteins in Interfaces in Plasma, *Biofouling*, **4**, 81 (1991).
Wojciechowski, P., and J. L. Brash, "A Computer Simulation for the Study of Macromolecular Adsorption with Special Applications for Single-Component Protein Adsorption," *J. Colloid Interf. Sci.*, **140**, 239 (1990).
Wojciechowski, P., and J. L. Brash, "The Vroman Effect in Tube Geometry: The Influence of Flow on Protein Adsorption Measurements," *J. Biomater. Sci. Poly. Ed.*, **2**, 203 (1991).
Wojciechowski, P., P. ten Hove, and J. L. Brash, "Phenomenology and Mechanism of the Transient Adsorption of Fibrinogen from Plasma (Vroman Effect)," *J. Colloid Interf. Sci.*, **111**, 455 (1986).
Yan, F., and P. Dejardin, "Kinetics of Fibrinogen Adsorption from Solution Flowing Through Polymer Hollow Fibers," *Langmuir*, **7**, 2230 (1991).
Yang, J. D., "Computational and Experimental Mass Transfer in Electrochemical Systems," PhD Thesis, Columbia Univ., New York (1997).

Manuscript received Mar. 27, 1997, and revision received Oct. 15, 1997.